Supplementary information

Method for Figure S1: AI-Generated Structural Representation Details

To provide a more intuitive visualization of the nano-Zn-Mg-Mn-Fe composite, we generated a digitally reconstructed structural illustration (Figure S1) using a combination of experimental SEM images and XRD diffraction data as input references for an AI-based visual modeling tool.

Input Data and Preparation

- SEM Micrographs: The raw SEM images (Figure S1, side panels) were obtained at ×50,000 and ×100,000 magnifications using a field emission scanning electron microscope (FESEM, JEOL JSM-7610F). These images revealed particle size ranges and aggregation morphology but lacked clarity in fine structure due to the dominance of light elements (Zn, Mg, Mn), which exhibit low electron contrast.
- XRD Pattern: X-ray diffraction data were collected using Cu Kα radiation (λ = 1.5406 Å) over a 2θ range of 10°–80°. Peaks corresponding to ferrite spinel structures and metal oxide phases of Zn, Mg, Mn, and Fe were confirmed using standard JCPDS files. Crystallite size was estimated using the Debye–Scherrer equation and determined to be in the range of 5–10 nm.
- Color and Elemental Attribution: Elemental color coding in the central model was based on standard material representations used in scientific visualizations:
    - Zinc – bluish-gray
    - Magnesium – silver-white
    - Manganese – grayish-pink
    - Iron – metallic gray
    -

AI Model and Image Generation Process:

- Platform Used: The AI-based visual model was generated using OpenAI's DALL·E tool (2024 version),(1) guided by a custom prompt based on SEM morphology, particle size (2–10 nm), elemental composition, and XRD-inferred structure.
- Prompt Example: *"Visualize a porous nanocomposite material composed of Zn, Mg, Mn, and Fe oxides. The structure should include spherical and irregularly shaped particles 2–10 nm in diameter, aggregated into clusters with high surface area. Use color coding for elements (Zn: bluish-gray, Mg: silver-white, Mn: pink-gray, Fe: metallic gray). Reflect structure consistent with ferrite phase as suggested by XRD pattern."*
- Model Training Note: As the DALL·E model is externally trained and not developed by the authors, it was used only to artistically render the structural features based on accurate experimental data. The representation is intended as a visual interpretation, not a crystallographic model.

Validation and Usefulness:

- While the image is not a replacement for high-resolution structural data (e.g., HRTEM or tomography), it was generated to support the interpretation of particle size, aggregation pattern, and material complexity inferred from SEM and XRD. It enhances communication of nanoscale morphology for readers in a visually accessible way.

- We acknowledge the limitations of generative AI and have made clear in the figure legend and supplementary file that this model is illustrative and based on empirical inputs rather than direct measurement.

Result and Discussion

The SEM images (Figure S1) provide a clearer view of the material's overall architecture, although detailed structural properties could not be resolved. This is likely due to the presence of light elements (Zn, Mg, and Mn) that have low electron scattering contrast, making it challenging to achieve sharp imaging. As a result, the electron diffraction signal could not provide sufficient contrast to clearly resolve individual nanoparticles, especially given their small size and thinness. However, a combination of TEM and SEM images together with XRD data, could be used as inputs into an AI model to generate material structure information (Figure S1).

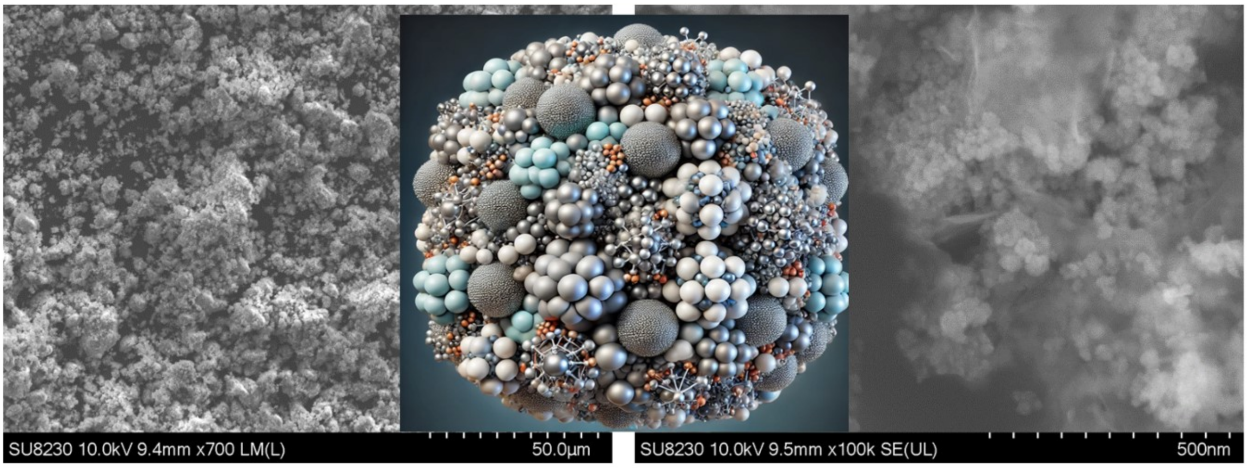

Figure S1. A detailed representation of the Nano-Zn-Mg-Mn-Fe composite using SEM images, illustrating (AI modelled) highly porous and aggregated clusters of spherical and irregular nanoparticles ranging from 2-10 nm in size. The central image highlights the composite's natural color-coded elements: zinc (bluish-gray), magnesium (silver-white), manganese (grayish-pink), and iron (metallic gray), providing a clearer view of the nanoparticle composition. The SEM images on the sides reveal the porous and complex aggregation of the nanoparticles, reflecting the structural characteristics of the composite and its potential for enhanced surface area and reactivity.

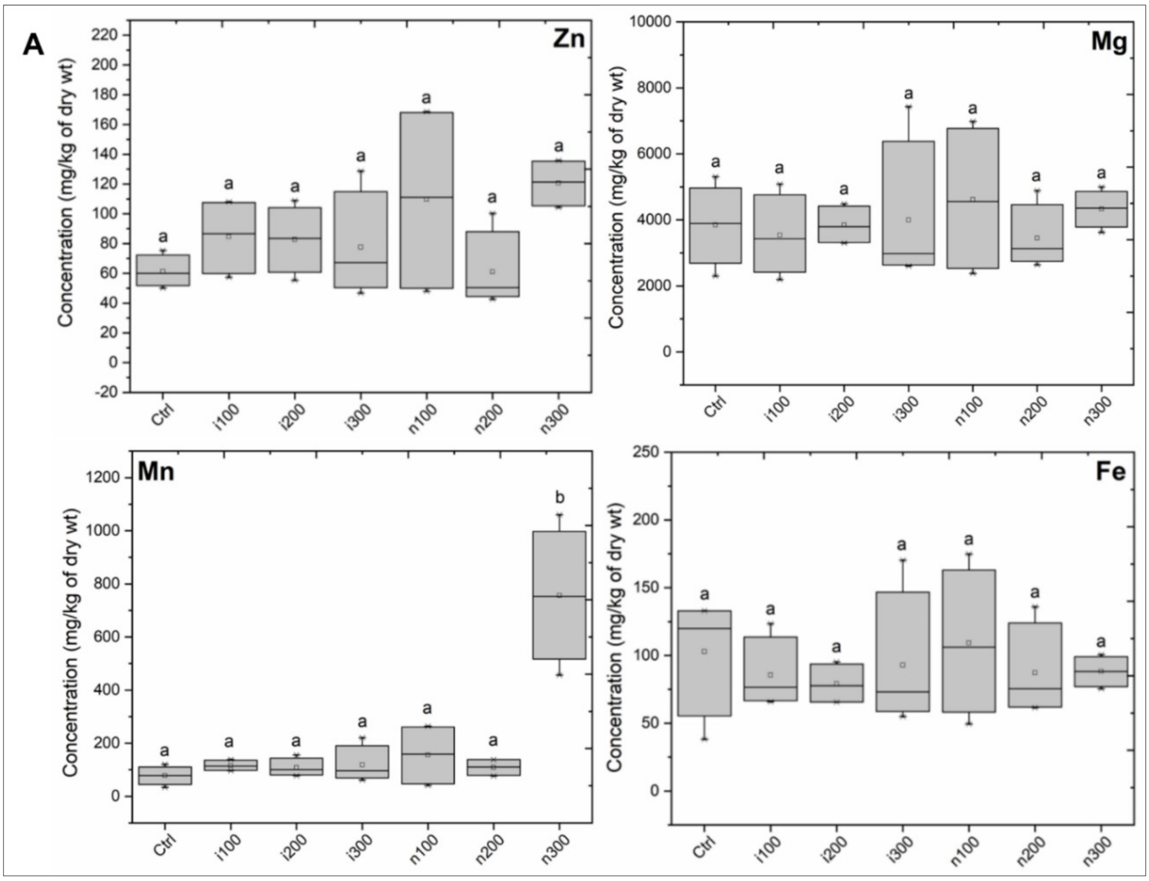
A
Zn
Mg
Mn
Fe
Concentration (mg/kg of dry wt)
Ctrl
i100
i200
i300
n100
n200
n300

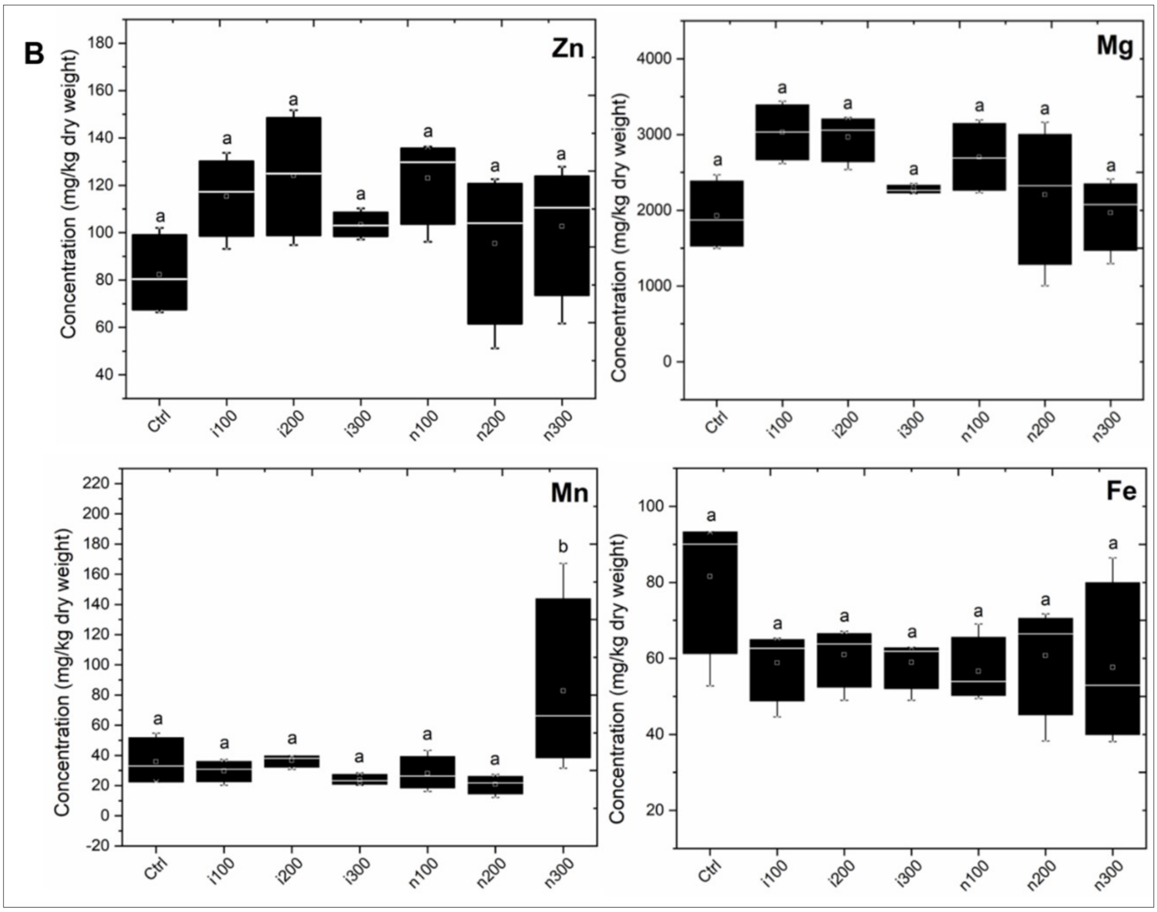
B
Zn
Mg
Mn
Fe
Concentration (mg/kg dry weight)
Ctrl
i100
i200
i300
n100
n200
n300

Figure S2. Elemental concentrations of Zn, Mg, Mn, and Fe in **lettuce leaves (A) and lettuce roots (B) measured under normal light exposure (LED)**, two weeks after treatment with water (control- untreated), ionic mixture (100, 200, 300 mg/L), and nano-Zn-Mg-Mn-Fe composite (100, 200, 300 mg/L) is presented. Statistically significant differences between treatments are indicated by different letters (Tukey's test, $p < 0.05$).

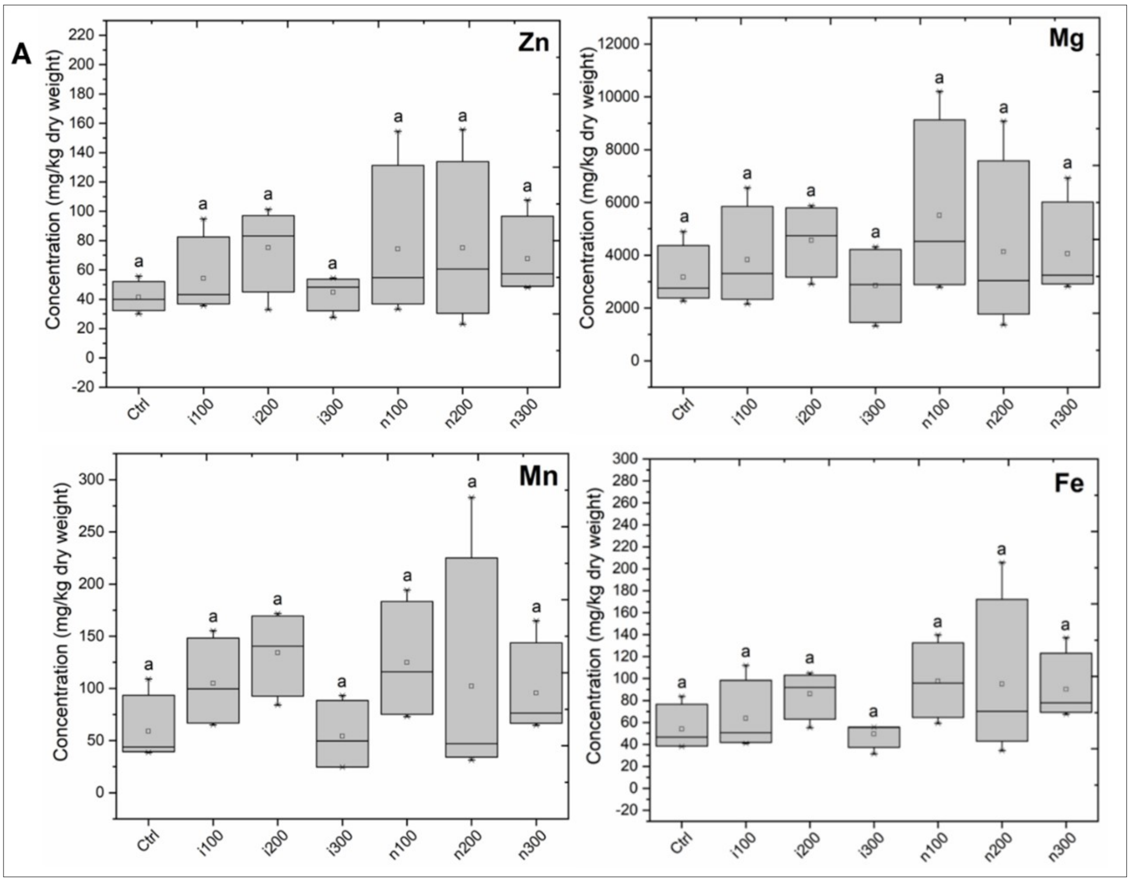
A
Zn
Mg
Mn
Fe
Concentration (mg/kg dry weight)
Ctrl
i100
i200
i300
n100
n200
n300
a

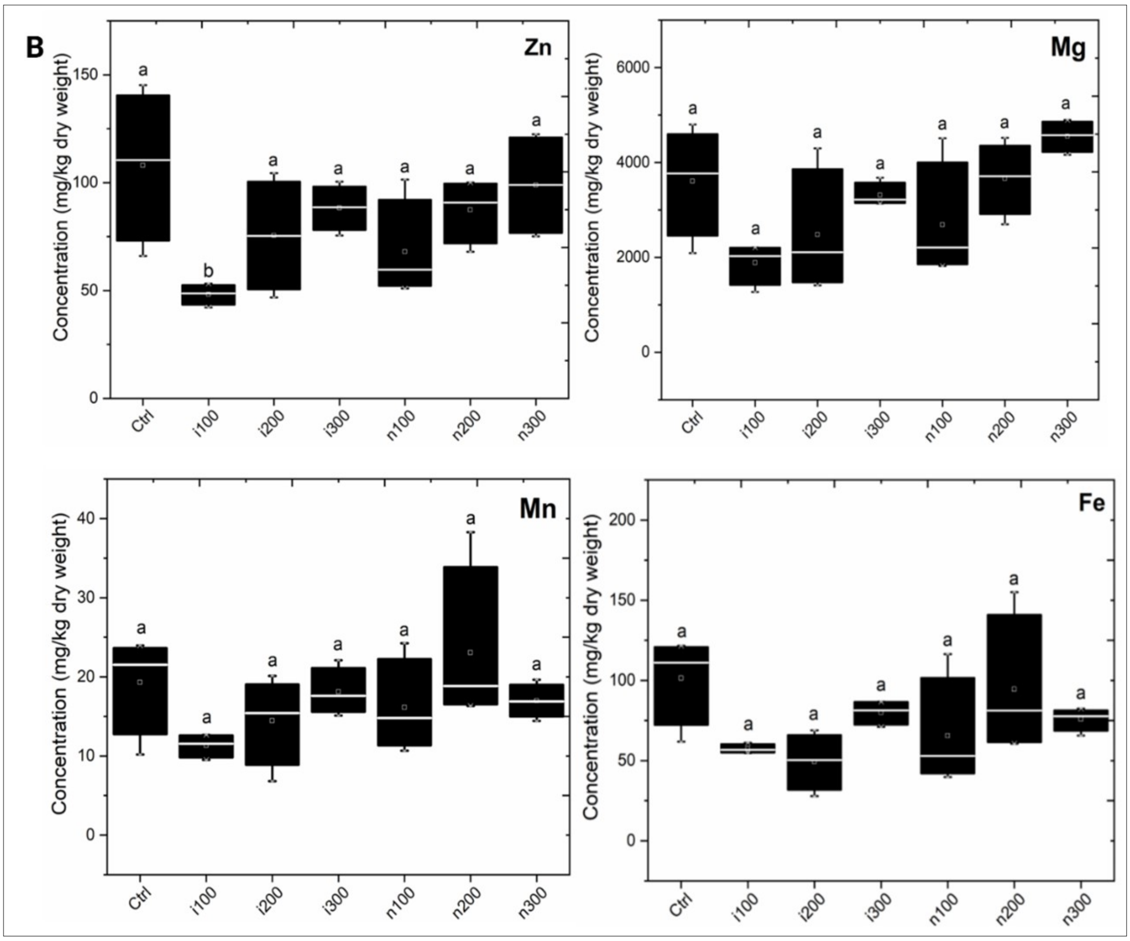
B
Zn
Mg
Mn
Fe
Concentration (mg/kg dry weight)
Ctrl
i100
i200
i300
n100
n200
n300
a
b

Figure S3. Elemental analysis **after UV exposure** of **lettuce leaves (A) and lettuce roots (B)** two weeks of post-treatment with water (control/untreated), ionic mixture (100, 200, 300 mg/L), and Nano-Zn-Mg-Mn-Fe composite (100, 200, 300 mg/L) is presented. Different letters above the boxplots indicate statistically significant differences between treatments (Tukey's test, $p < 0.05$).

Nutrient profile analysis of key elements (LED and UV exposed)

The elemental analysis (ICP-OES) of macro and secondary nutrients (K, Ca, S, P, Na) in lettuce treated with an ionic mixture or nano-Zn-Mg-Mn-Fe composite after exposure to LED and UV light was determined (Figure S4). The analysis of nutrient concentrations in LED-exposed leaves (Figure S4 A) revealed that the 300 mg/L nano-Zn-Mg-Mn-Fe composite significantly enhanced Ca and S accumulation, with Ca reaching 89.51 mg/kg and S increasing to 12.97 mg/kg dry weight, compared to the control (64.48 mg/kg dry weight for Ca and 11.89 mg/kg dry weight for S). Potassium levels were comparable between the 300 mg/L nanocomposite treatment (250.59 mg/kg dry weight) and the control (251.10 mg/kg dry weight), while the ionic mixture treatments showed reduced K accumulation, ranging from 183.27 to 193.45 mg/kg dry weight. Phosphorus (P) concentrations were relatively stable across all treatments, with a slight increase observed in the 300 mg/L nanocomposite treatment (41.06 mg/kg dry weight) compared to the control (33.84 mg/kg dry weight).

The analysis of nutrient concentrations in LED-exposed roots (Figure S4. B) revealed significant variations across treatments. Calcium (Ca) and phosphorus (P) levels were highest in plants treated with the 300 mg/L nano-Zn-Mg-Mn-Fe composite, reaching 65.37 mg/kg dry weight and 12.00 mg/kg dry weight, respectively, compared to the control (37.42 mg/kg dry weight for Ca and 9.18 mg/kg dry weight for P). Potassium (K) accumulation was also significantly enhanced in the 300 mg/L nanocomposite treatment (134.10 mg/kg dry weight), showing a substantial increase compared to the control (136.22 mg/kg dry weight). Sulfur (S) levels exhibited a consistent trend, with the 300 mg/L nanocomposite treatment reaching 21.68 mg/kg dry weight, higher than the control (24.59 mg/kg dry weight). Sodium (Na) concentrations varied across treatments, with the highest value observed in the 300 mg/L nanocomposite treatment (33.27 mg/kg dry weight).

Under UV exposure (Figure S4. C), nutrient accumulation patterns in leaves showed distinct differences compared to those under LED conditions. While potassium (K) levels in UV-exposed leaves increased significantly in the 300 mg/L ionic mixture treatment (137.51 mg/kg dry weight), this was notably higher than the corresponding LED treatment (125.04 mg/kg dry weight), suggesting enhanced K uptake under UV stress. Similarly, calcium (Ca) levels in the 100 mg/L nanocomposite treatment (54.30 mg/kg dry weight) were markedly higher under UV exposure compared to LED conditions (39.90 mg/kg dry weight), indicating a stronger response to UV-induced stress. Phosphorus (P) concentrations also showed a notable increase under UV, particularly in the 300 mg/L ionic mixture treatment (24.85 mg/kg dry weight), which surpassed the levels observed in the LED treatments (21.64 mg/kg dry weight). Sulfur (S) levels followed a similar trend, with the 300 mg/L ionic mixture treatment under UV exposure (7.09 mg/kg dry weight) exceeding its LED counterpart (6.48 mg/kg dry weight). These results highlight that UV exposure amplified nutrient uptake in specific treatments, potentially due to increased plant stress responses driving nutrient demand.

The nutrient concentrations in UV-exposed roots exhibited distinct trends across treatments. Under UV exposure (Figure S4. D), nutrient accumulation in roots exhibited significant differences compared to LED-exposed roots. Sodium (Na) levels in UV-exposed roots showed a slight decrease in the 300 mg/L nano-Zn-Mg-Mn-Fe composite treatment (34.63 mg/kg dry weight) compared to the LED treatment (36.71 mg/kg dry weight), suggesting reduced Na uptake under UV conditions. Phosphorus (P) accumulation was markedly higher under UV in the 300 mg/L nanocomposite treatment (45.38 mg/kg dry weight) compared to the LED treatment (23.77 mg/kg dry weight), indicating an enhanced P response to UV stress. Sulfur (S) levels remained relatively stable between UV and LED conditions, with the highest levels observed in the control (11.29 mg/kg dry weight for UV, 11.89 mg/kg dry weight for LED). Calcium (Ca) levels in the 300 mg/L nanocomposite treatment were slightly lower under UV exposure (26.34 mg/kg dry weight) compared to LED conditions (41.19 mg/kg dry weight), suggesting a reduction in Ca uptake under UV stress. Potassium (K) levels, however, showed an opposite trend, with the 300 mg/L ionic mixture treatment under UV exposure (56.80 mg/kg dry weight) surpassing the corresponding LED treatment (50.36 mg/kg dry weight). These comparisons highlight the differential impacts of UV and LED exposure on nutrient uptake and suggest that UV-induced stress selectively influences the accumulation of specific nutrients in roots.

The nutrient profile analysis reveals distinct differences in nutrient uptake patterns in lettuce plants exposed to LED and UV light when treated with either an ionic mixture or a nano-Zn-Mg-Mn-Fe composite. Potassium (K), essential for stress response,(2) photosynthesis, and enzyme activation, exhibited enhanced uptake in both leaves and roots across most treatments. Under LED exposure, the 300 mg/L nano-Zn-Mg-Mn-Fe composite significantly increased K levels, while under UV exposure, the 300 mg/L ionic mixture treatment demonstrated superior K accumulation in roots, highlighting a differential response to lighting conditions. This suggests that while the nanocomposite supports consistent and efficient K translocation, the ionic mixture may facilitate more rapid K absorption under UV stress. Phosphorus (P), a crucial macronutrient for energy transfer and metabolic processes,(3) showed notable increases under UV exposure, particularly with the 300 mg/L nanocomposite treatment, which doubled P accumulation in roots compared to LED exposure. This highlights the nanocomposite's role in enhancing P bioavailability under UV stress. Calcium (Ca),(4) critical for cell wall stabilization and signaling, remained stable across most treatments, though a marginal increase in Ca levels was observed in LED-exposed roots treated with the 300 mg/L nanocomposite, suggesting slight improvements but significantly in Ca bioavailability under LED conditions. Sulfur (S), essential for protein synthesis and chloroplast function,(5) showed a marked increase in leaves treated with the 300 mg/L ionic mixture under both LED and UV exposure, suggesting its involvement in mitigating UV-induced stress. This response could be attributed to the role of sulfur in the biosynthesis of glutathione, a critical component of the glutathione pathway, which plays a central role in managing oxidative stress and enhancing both abiotic and biotic stress tolerance.(6) The upregulation of this pathway may contribute to the observed stress mitigation effects, underscoring the importance of sulfur in maintaining cellular redox balance under UV stress conditions. Sodium (Na), while non-essential, plays a role in osmoregulation.(7) Its accumulation was significantly higher in roots under UV exposure treated with the 300 mg/L nanocomposite, suggesting potential benefits for osmotic balance and stress adaptation, though excessive Na uptake could pose phytotoxic risks. The results highlight that while the ionic mixture may rapidly supply nutrients such as K and S, the nanocomposite supports sustained and targeted nutrient delivery, making it a promising candidate for optimizing plant nutrition and enhancing resilience under diverse lighting conditions.

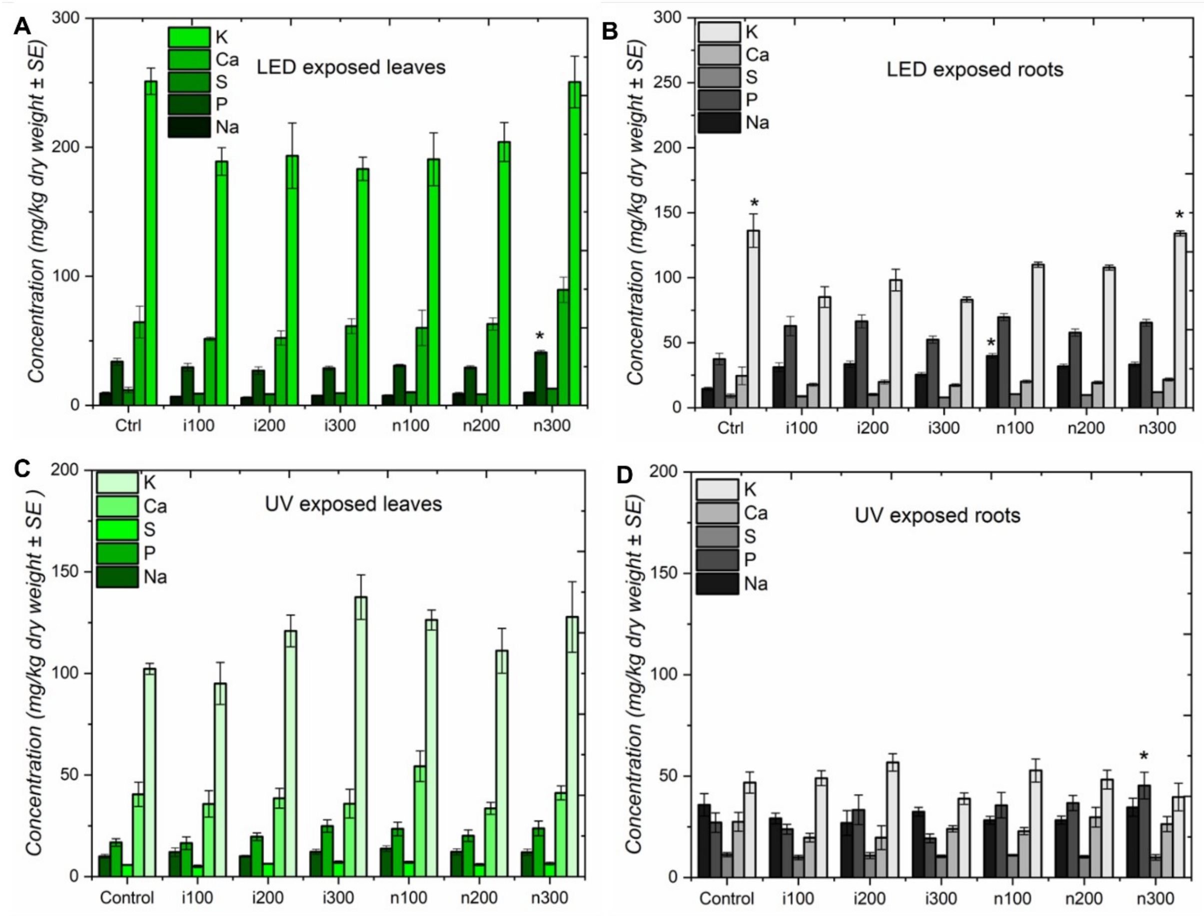

Figure S4. Nutrient profile analysis of key elements (K, Ca, S, P, Na) in lettuce plants under different light conditions: normal LED light (Panels A and B) and UV-stress conditions (Panels C and D). Plants were treated with Control (untreated), Ionic mixture (100, 200, 300mg/L), and Nano-Zn-Mg-Mn-Fe composite (100, 200, 300 mg/L) followed by two weeks of post-foliar application. **Panel A:** Element concentrations in leaves exposed to LED light; **Panel B:** Element concentrations in roots exposed to LED light; **Panel C:** Element concentrations in leaves exposed to UV light; **Panel D:** Element concentrations in roots exposed to UV light. The Y-axis represents element concentrations, expressed either in ppm ± SE or potentially in mg/kg of dry weight, depending on the specific context of the analysis. Different letters indicate statistically significant differences between treatments, while asterisks (*) denote significant changes compared to the control (Tukey's test, $p < 0.05$). All values are expressed in mg/kg dry weight unless otherwise stated

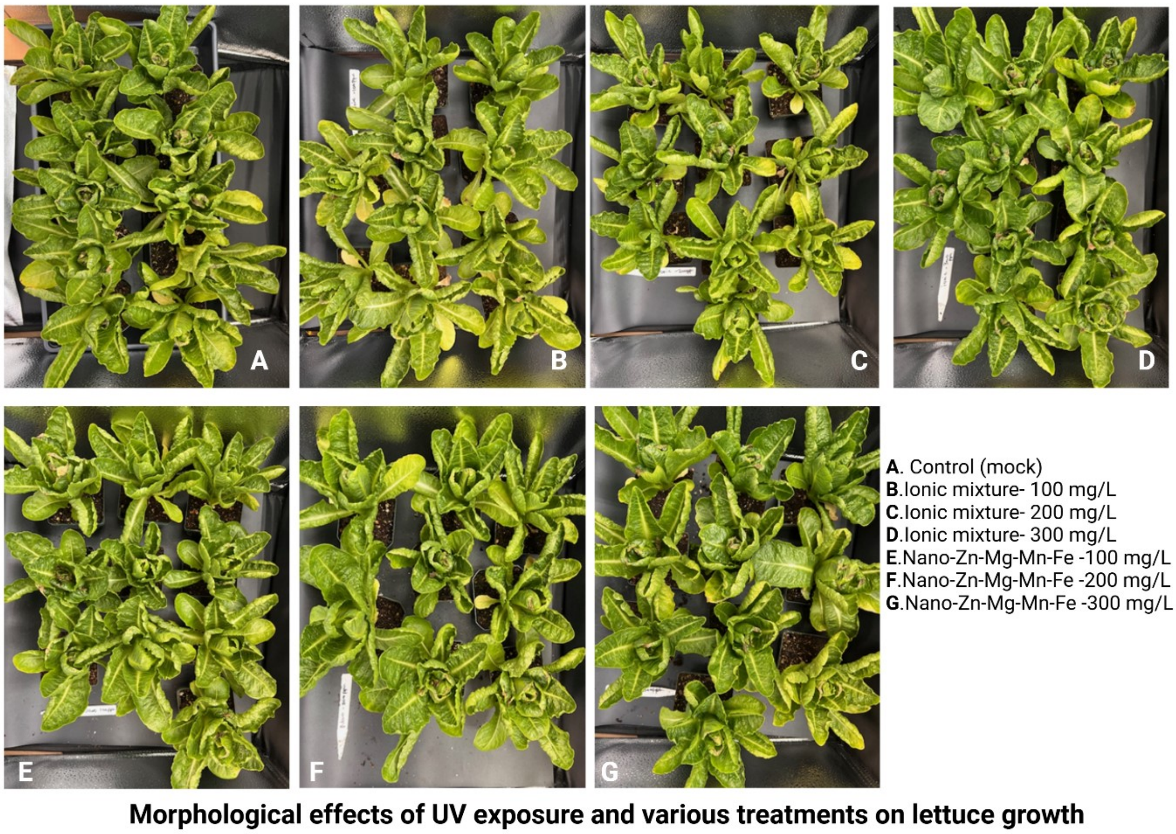

Figure S5. Digital images showing the morphological effects of UV exposure on lettuce plants two weeks after treatment with various concentrations (100, 200, 300 mg/L) of the ionic mixture or nano-Zn-Mg-Mn-Fe composite. This set of images illustrates the comparative morphological responses of lettuce plants to UV stress and subsequent treatments. These treatments induced distinct differences in plant morphology, including leaf tip burning, yellowing, and growth retardation, highlighting the protective or growth-enhancing effects of the formulations under UV stress. The control plants represent the baseline morphological state, exhibiting severe symptoms typical of UV stress in the absence of any treatment. In contrast, the treated groups displayed varying degrees of improvement or maintenance of healthy growth, depending on the concentration and type of formulation applied.

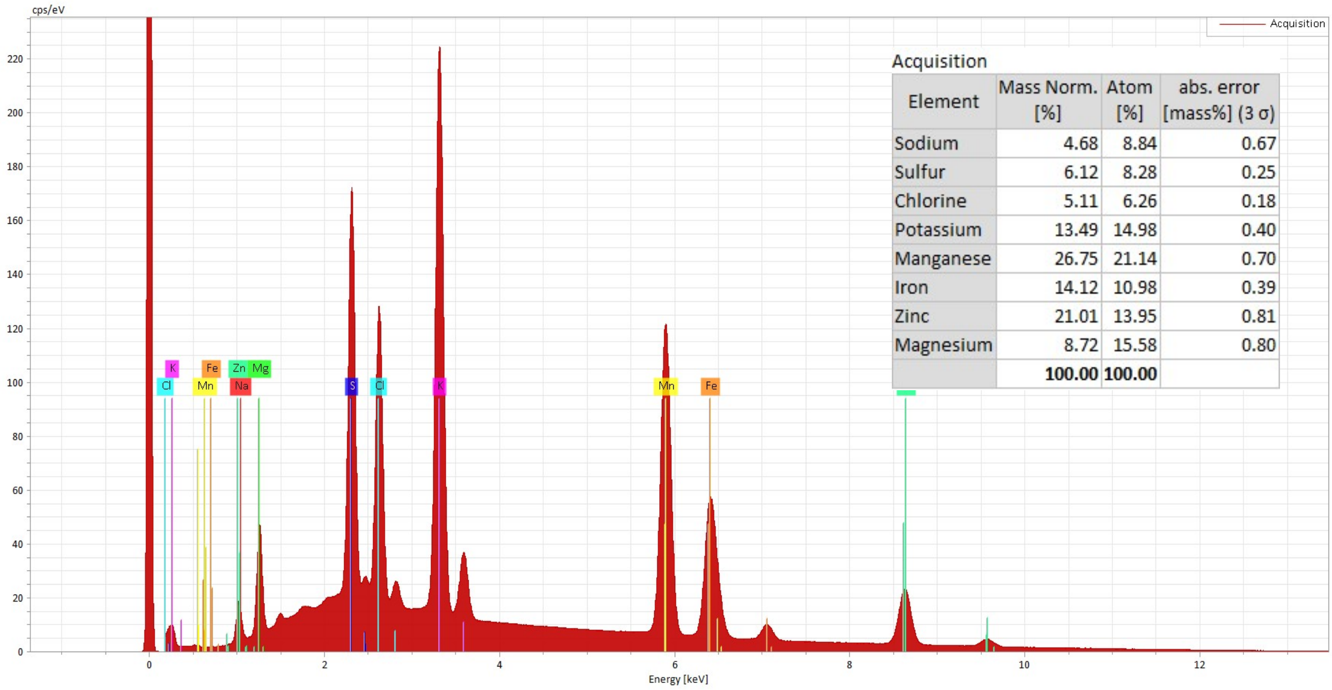

Figure S6. SEM-EDX elemental profile of the nano-Zn-Mg-Mn-Fe composite showing the normalized mass percentage and atomic percentage of elements, including sodium, sulfur, chlorine, potassium, manganese, iron, zinc, and magnesium. The corresponding error for each element (3σ) is also provided.

References cited

1. ChatGPT [Internet]. [cited 2025 Apr 4]. Available from: https://chat.openai.com/

2. Wang M, Zheng Q, Shen Q, Guo S. The critical role of potassium in plant stress response. Int J Mol Sci [Internet]. 2013 Apr 2;14(4):7370–90. Available from: http://dx.doi.org/10.3390/ijms14047370

3. Khan F, Siddique AB, Shabala S, Zhou M, Zhao C. Phosphorus plays key roles in regulating plants' physiological responses to abiotic stresses. Plants [Internet]. 2023 Aug 3;12(15). Available from: http://dx.doi.org/10.3390/plants12152861

4. Thangavelu RM, da Silva WL, Zuverza-Mena N, Dimkpa CO, White JC. Nano-sized metal oxide fertilizers for sustainable agriculture: balancing benefits, risks, and risk management strategies. Nanoscale [Internet]. 2024 Nov 7;16(43):19998–20026. Available from: http://dx.doi.org/10.1039/d4nr01354a

5. Li Q, Gao Y, Yang A. Sulfur homeostasis in plants. Int J Mol Sci [Internet]. 2020 Nov 25;21(23):8926. Available from: http://dx.doi.org/10.3390/ijms21238926

6. Noctor G, Mhamdi A, Chaouch S, Han Y, Neukermans J, Marquez-Garcia B, et al. Glutathione in plants: an integrated overview. Plant Cell Environ [Internet]. 2012 Feb;35(2):454–84. Available from: http://dx.doi.org/10.1111/j.1365-3040.2011.02400.x

7. Yamaguchi T, Hamamoto S, Uozumi N. Sodium transport system in plant cells. Front Plant Sci [Internet]. 2013 Oct 17;4:410. Available from: http://dx.doi.org/10.3389/fpls.2013.00410